Enhanced High Harmonic Generation from Xe, Kr, and Ar in a Capillary Discharge

B.A. Reagan,[1] T. Popmintchev,[2] M.E. Grisham,[1] D.M. Gaudiosi,[2] M. Berrill,[1] O. Cohen,[2] , B. C. Walker[3], M.M. Murnane,[2] J.J. Rocca,[1] and H.C. Kapteyn[2]

National Science Foundation ERC for Extreme Ultraviolet Science and Technology

[1]Department of Electrical and Computer Engineering, Colorado State University, Fort Collins, CO 80523-1373, USA

[2]Department of Physics and JILA, University of Colorado and National Institute of Standards and Technology, 440 UCB, Boulder, CO 80309-0440, USA

[3]Department of Physics and Astronomy, University of Delaware, 223 Sharp Laboratory, Newark, DE 19716, USA

(Received 26 February 2007)

Abstract

We report the use of a pre-ionized medium created by a capillary discharge to extend the cutoff photon energy in high-order harmonic generation. The observed enhancements result from a combination of reduced ionization energy loss and reduced ionization-induced defocusing of the driving laser. We observe harmonic emission from Xe up to a photon energy of 160 eV, and we extend this technique to other noble gases for the first time, observing photons with energies up to 170 eV from Kr, and 275 eV from Ar. The discharge plasma also provides a means to spectrally tune the harmonics by tailoring the initial level of ionization of the medium. Our results are interpreted using a hydrodynamic / atomic physics model of the discharge plasma. This work demonstrates that capillary discharges are a versatile and general method for generating harmonics, in particular from ions. Finally, this approach should be scaleable to efficiently generate coherent light at much shorter wavelengths, in combination with novel phase-matching techniques.

PACS numbers: 42.65.Ky, 42.65.Re, 52.35.Mw, 52.38.-r, 52.40.Fd

I. Introduction

High-order harmonic generation (HHG) has proven to be a useful source of coherent extreme ultraviolet (EUV) and soft x-ray radiation. Several applications of HHG light have been demonstrated to date, such as the investigation of surface dynamics [1, 2], probing static molecular structure and internal molecular dynamics [3, 4], the study of nonlinear optic effects at EUV wavelengths [5], as well as holographic [6] and photoacoustic [7] imaging. When a medium is illuminated by an intense laser field, odd-order harmonics of the fundamental laser are generated. The highest photon energy that can be produced through this process is predicted by the cutoff rule to be $h\nu_{max} = I_p + 3.17U_p$, where I_p is the ionization potential of the target atom and U_p is the ponderomotive energy of the liberated electron in the laser field [8]. ($U_p=E^2/4\omega^2$ in atomic units where E is the peak of the laser electric field with frequency ω). In principle with long wavelength or high field lasers, $h\nu_{max}$ may be as high as 6keV before relativistic effects suppress rescattering and HHG [9].

To date however, for many experiments the highest harmonic photon energies observed have not been limited by the available laser intensity, but rather by the ionization of the nonlinear medium by the driving laser. The depletion of neutrals does not terminate the harmonic emission since high harmonics may also be generated from ions. Rather, the electron density from photoionization refractively defocuses the driving laser, reducing the peak laser intensity and consequently the highest harmonic photon energy observed. Moreover, the resulting plasma imparts different phase velocities to the driving laser and the HHG light, which results in poor phase-matching and conversion efficiency. Finally, the loss of the laser energy due to photoionization limits the length in the medium over which a high peak intensity can be maintained.

In past experiments, extremely short laser pulses, [10] and target atoms with high ionization potential [11] were employed to obtain the highest possible photon energies, since both of these characteristics allows neutral atoms to survive to higher laser intensities. Seres *et al.* recently demonstrated that harmonics with photon energies up to 3.5 keV can be obtained by using intense 12 fs laser pulses focused into a He gas cell [12]. Although nonadiabatic effects may help to ameliorate the very short coherence length in these experiments,[13] the flux is nevertheless very low. Another method to extend harmonics to higher photon energies is to generate harmonics from ions rather than neutral atoms [14, 15]. Ions have higher ionization potentials than neutrals and therefore ionize at much higher laser intensities. Gibson *et al.* demonstrated that significantly higher harmonics, up to 250 eV, can be generated from Ar ions by confining the driving laser beam in a gas-filled hollow waveguide. The use of a hollow waveguide greatly reduces ionization-induced defocusing, allowing a significant extension of the cutoff photon energy.

Harmonic generation in a preformed plasma with a tailored density profile can further enhance harmonic generation from ions. The use of preformed plasma waveguides for HHG has been previously proposed [16, 17], but was not demonstrated experimentally until recently. Capillary discharges provide a convenient way to generate plasma waveguides with a tailored degree of ionization in numerous gases and vapors [17-20]. In recent work, we demonstrated that a significant extension of the HHG cutoff in Xe can be obtained using a capillary discharge to produce a preformed, fully-ionized plasma [21]. In that work, the range of photon energies generated in Xe was extended to ~150 eV, well above the highest previously-observed value of ~70 eV [22].

In this paper we expand our previous results by extending high harmonic generation from Xe, Kr, and Ar using a capillary discharge, to photon energies well beyond what have been previously observed. Harmonic emission from Kr and Ar in a discharge medium is demonstrated here for the first time. Our results show that in all three gases, the cutoff energy for HHG is enhanced in a capillary discharge beyond what is possible in a capillary without the discharge. By combining experimental measurements of the harmonic spectrum and of the transmitted laser pulse with a hydrodynamic model of the discharge plasma, we show HHG emission from ions is extended and enhanced because of improved laser transmission through the waveguide, mainly due to reduced ionization-induced defocusing and decreased ionization losses. Moreover, the ionized medium created by the discharge also provides a method to spectrally tune the harmonics by tailoring the initial level of ionization of the medium. We conclude by discussing the present limitations of this method, notably the fact that the process is still not well phase matched, and evaluate the prospects for using new techniques that could further extend the range of photon energies that can be efficiently generated. This work clearly shows that the use of capillary discharges provides a versatile and general method for generating harmonics from ions.

II. Experimental Setup

The experimental setup consists of an ultrafast laser system to generate the high intensities and an adjustable capillary discharge to create the interaction region. The capillary discharge setup used in these experiments is shown in Fig. 1. Gas was injected into a 250 μm inner diameter, 50 mm long quartz capillary through two 1mm holes drilled approximately 3 mm from the ends of the capillary. The short sections between the holes and the entrance of the capillary allow a constant gas pressure to be maintained over the length of the capillary while

using the chambers preceding and following the discharge for differentially pumping (~10^{-5} Torr). The discharge current was injected through electrodes placed at the entrance and near the exit of the capillary. The discharge circuit consisted of a storage capacitance of 9.9 nF and a series inductance of 100 μH. Current pulses were initiated using a thyratron switch. A ~10 mA DC simmer current was driven through the capillary to improve the uniformity of the plasma column and to reduce the jitter of the main current pulses. The discharge can operate at repetition rates up to 200 Hz before heat removal becomes a significant problem. Improved cooling of the discharge head would allow operation at kHz repetition rates. The entire capillary discharge is very compact, measuring 10 cm in diameter and 10 cm in length, allowing it to be mounted on a stage with translation in two directions and rotation on two axes, simplifying alignment to the injected laser pulses. Within a selected range of pressures and currents, the dominant heating of the plasma in the axial regions of the capillary creates a concave electron density profile that results in an index waveguide [16, 17, 19, 20].

The Ti:sapphire CPA system used in the experiments produced 22-30 fs FWHM duration pulses with energies up to 15 mJ at 10 Hz repetition rate. Laser pulses were focused onto the capillary discharge entrance with a f = 75 cm lens to a measured diameter of ~150 μm. The HHG signal exiting the waveguide was detected using a grazing incidence EUV spectrometer with an x-ray CCD detector. Silver and zirconium foils were used to reject the transmitted laser light, and silicon, boron, and aluminum filters were used for wavelength calibration of the EUV spectra. To facilitate alignment and to measure the energy and beam quality of the transmitted laser pulses, a removable mirror was placed between the discharge and the spectrometer.

III. Results

In the following, we discuss the extension of the high harmonic generation cutoff photon energies in Xe, Kr, and Ar, using a capillary discharge, to photon energies not previously observed using any approach. Previous work by *Gaudiosi et al.* [21] demonstrated high harmonic generation from Xe ions in a capillary discharge for the first time. In this work, by monitoring the harmonic output with and without the discharge, a dramatic extension of the harmonic cutoff, from 95 eV to 150 eV, was observed. In addition to extending the cutoff photon energy, the harmonic flux near the cutoff was enhanced by nearly two orders of magnitude. Also, the reduction of self-phase modulation resulted in the observation of clearly resolved harmonic peaks up to 85 eV.

In this work, more optimal laser coupling into a larger diameter capillary resulted in further extension of the harmonic cutoff in Xe, from 150eV in our past work to photon energies above 160 eV. Also, because the harmonic cutoff is extended due to reduced ionization-induced refraction and better guiding of the laser, the harmonic signal near cutoff is also enhanced due to increased laser intensity and ionization rates. We observe enhancement of the near-cutoff harmonics by an order of magnitude near 120 eV. This enhancement is less than observed in our past work (two orders of magnitude near 90 eV), because the larger-diameter waveguide allows us to generate harmonics up to 120 eV in Xenon even without the discharge running. We also observed clear harmonic peaks, up to photon energies of 110 eV (Fig. 2a). This experiment used 10 mJ, 28 fs laser pulses focused into the discharge initially filled with 3 Torr of Xe. A higher discharge current (10 A) was employed in comparison with earlier experiments because of the larger inner diameter of the capillary - 250 μm versus 175 μm in [21].

Extension and enhancement of the cutoff harmonics were also demonstrated in Kr and Ar in the presence of a discharge. As seen in Figs. 2b and 2c, using a capillary waveguide without the discharge running, the HHG signal extends to 125 eV for Kr and 225 eV for Ar. When the discharge was used, the observed maximum photon energies were extended further, to 170 eV and 275 eV, respectively. Prior to these experiments, the highest photon energies generated from these two gases using an 800 nm driving laser were 70 eV [23] and 250 eV [14], respectively. In both cases, the emission was attributed to ions. Thus, the cutoff in Kr was extended by 100 eV while the cutoff in Ar was extended by 25 eV, compared with all past measurements. The discharge pulses used for these experiments had amplitudes of 12 A and 5 A for Kr and Ar, respectively. As well as extending the cutoff photon energy, the presence of the discharge also enhances the harmonic flux in Kr and Ar at high photon energies. The plasma defocusing and ionization loss are smaller in the case of Kr and Ar when compared to Xe; as a result, the enhancement of the HHG flux is less than in the case of Xe. Observation of increased emission from ions in a capillary discharge for all three gases demonstrates the use of a discharge as the nonlinear medium is a general method for generating high harmonics from ions and for extending the cutoff to higher photon energies.

In the case of Ar, the characteristics of the plasma column were optimized for maximum HHG cutoff by adjusting the gas pressure, the delay of the laser pulse with respect to the rising edge of the discharge current pulse, the driving laser intensity and the amplitude of the discharge current pulse. All of the HHG spectra from Ar were measured using two 200 nm thick silver filters, which only transmit photons with energy above ~110 eV. Silicon and boron filters, which have sharp absorption edges at 99.9 eV and 188.4 eV, respectively, were used for calibration of the spectrometer.

Fig. 3 shows the HHG signal in Ar for various delay times, τ, between the onset of the discharge current pulse and the arrival the driving laser. Even before the discharge pulse is initiated, there is a small enhancement of the HHG flux and cutoff photon energy when compared with the spectrum taken in the capillary waveguide without the discharge on. This is due to reduced photoionization-induced refraction of the driving laser associated with the small DC simmer current. At the optimum delay of τ = 2 μs, the HHG spectrum near cutoff is enhanced and extends to even shorter wavelengths of 275 eV.

Our data clearly shows that by creating a preformed, ionized medium, the discharge reduces ionization-induced refraction losses of the laser, making it possible to maintain a high laser intensity over a long interaction length. The higher laser intensity extends the harmonic cutoff and increases the ionization rate, leading to the generation of brighter harmonics as observed experimentally. The reduced refraction of the laser is shown in Fig. 4, where the pulse energy is varied in the capillary, with and without the discharge running. In these data, a peak laser intensity of 2-3x10^{15} W/cm^2 was used to generate photon energies > 200 eV in Ar. Without the discharge running, the HHG spectrum does not change significantly as the laser pulse energy is increased from 9 mJ to 11 mJ, indicating that the peak intensity is clamped by photoionization-induced defocusing. However, when the discharge is present, there is a large enhancement in HHG flux because of the higher laser intensity and increased photoionization as the driving pulse energy is increased.

Figure 5 plots harmonic emission from Ar in the photon energy range >100 eV, where, according to the Ammosov, Delone, and Krainov (ADK) model of tunnel ionization [24], HHG emission up to ~170 eV can originate from ionization either of neutrals or of ions (Fig. 8). Here, the higher level of ionization of the discharge-created plasma reduces the density of neutral

atoms that have higher nonlinear susceptibility. Increasing ionization also decreases the coherence length between the driving laser and the harmonics, thereby reducing the harmonic flux when the discharge is running. This is in contrast to higher photon energies (>200 eV), which are enhanced in the presence of the discharge. These effects can be seen in Fig. 5, as the discharge current is varied from 5 to 15 A. Comparing with the spectra obtained with and without the discharge, the presence of the discharge clearly reduces ionization-induced refraction, even at the minimum current of 5 A. However, as the current is further increased, the HHG flux at ~100 eV is reduced due to the lower ionization rate and the shorter coherence length associated with a higher overall level of ionization. A similar drop in the HHG flux in the low energy range is observed in the case of harmonic emission from Kr and Xe in the discharge (Fig 2), although higher currents are needed to obtain a similar degree of ionization in Ar (>15 A) compared with Xe (10 A). Again, the flux at high photon energies is not decreased, where ADK calculations show that these harmonics are only generated at times during the laser pulse when the plasma is completely ionized. These harmonics have similar coherence lengths regardless of whether the plasma is completely ionized by the laser or by the discharge. Finally, measurements of the laser energy transmitted through the discharge indicate that the cutoff photon energy should extend to > 400 eV for the estimated laser intensity of 2.3×10^{15} W/cm^2 used in these experiments.These data thus indicate that any further extension of the cutoff in Ar is primarily limited by the large plasma-induced phase mismatch between the fundamental and harmonic waves. These macroscopic effects are discussed in more detail in the following section.

IV. Discussion

In order to understand in detail the reported results, we developed a computer simulation of the capillary discharge plasma using a one dimensional hydrodynamic code [25]. This approach is appropriate given the very high aspect ratio of the capillary. The code solves the hydrodynamic equations in combination with a collisional-radiative model that computes the atomic populations using atomic rates from the FAC [26] and ADAS [27] codes, and multi-cell radiation transport [28].

A. Capillary Discharge Plasma Model

Fig. 6 shows the computed spatio-temporal evolution of the plasma parameters for a 10 A peak current pulse in xenon. The measured temporal profile of the current pulse used to obtain the results in Fig. 2a was used for this simulation, and is shown in Fig. 6a. As can be seen from Fig. 6b, the plasma in the central region of the capillary is rapidly ionized to a mean ion charge Z_m of ~1 and remains predominately singly ionized for several microseconds. At the delay for which the harmonic spectrum of Fig. 2 was obtained (τ = 1.5 μs) the plasma is essentially completely singly ionized. Moreover, calculations of optical field ionization rates using the ADK model [24] show that neutral Xe cannot survive to the intensities required for harmonic generation above ~80 eV. These two calculations lead us to conclude that the harmonic spectrum shown in Fig. 2a is generated overwhelmingly from Xe ions.

Fig. 6c shows the simulated electron temperature. During the current pulse the plasma is hottest in the center with the temperature decreasing radially, since maximum Ohmic heating occurs on axis and the walls of the capillary act as a heat sink. As initial pressure shockwaves are dampened and pressure equilibrium is established, this temperature profile leads to an electron

density profile that is minimum on axis and increases radially as shown in Fig. 6d. Fig. 6e shows the concave radial profile of the electron density at a delay of $\tau = 2\mu s$. This simulation predicts that under the conditions at which the spectrum of Fig. 2a was obtained, the discharge prepares a nonlinear medium that consists nearly entirely of singly ionized Xe. Additionally, the concave electron density profile of the plasma assists in guiding the beam and mitigates ionization induced defocusing.

In contrast, for the same current pulse in 6 Torr Ar, the model predicts that the electron density profile is not concave. The computed plasma parameters for Ar are shown in Fig. 7. Although the plasma achieves a similar electron temperature as the Xe case, the Ar plasma is not completely ionized. This is due to the significantly higher ionization potential of neutral Ar of 15.8 eV, compared with 12.1 eV for neutral Xe, and also the larger ion diffusion loss to the walls in Ar. Because not all of the neutral atoms are ionized at this current, the radial temperature difference leads to a radial variation in ionization. The increased ionization in the hot center of the discharge plasma flattens the electron density profile. Experimental measurements of laser beam propagation through the Ar plasma are discussed below and are consistent with this explanation.

To interpret the data of Fig. 5, we calculated the peak mean ionization of the Ar plasma as a function of discharge current (Fig. 7e). The discharge model predicts that the Ar plasma has a mean ion charge of about 0.3 for a peak discharge current of 5 A, which gradually increases, achieving and average ionization of $Z_m \sim 1$ at ~15 A. Relating the calculated level of ionization with the harmonic spectra of Fig. 5, we see that the flux of higher energy harmonics remains relatively unchanged for discharge currents above 5 A. This suggests that harmonics above 200 eV are created entirely from Ar ions. This scenario is supported by calculations of the ADK

ionization rates which show that no neutral Ar atoms remain by the time the laser is intense enough to generate these harmonics. In contrast, the lower energy harmonics, which can be generated from both neutral and singly ionized Ar, are initially enhanced at 5 A due to a 1.7 times higher laser intensity at the exit of the capillary when the discharge is turned on. Further increasing the discharge current reduces the harmonic signal most likely as a result of a combination of microscopic and macroscopic effects: a decrease in the ionization rates and a reduction in the coherence lengths. In a single atom picture, the harmonics at ~125 eV are generated more efficiently at the leading edge of the laser pulse near their threshold intensity, i.e. the intensity at which a given harmonic is at cutoff [29]. At 5 A discharge current, the higher laser energy transmitted through the fiber boosts the ionization rate, as seen in Fig. 8 b and d, thus enhancing the HHG flux. Since these harmonics are generated at time during the laser pulse in which the estimated mean ionization Z_m at the threshold is between ~0.75 (5 A) and ~1.0 (at 15 A), the pre-ionization by the discharge (from Z_m ~0.3 at 5 A to Z_m ~1.0 at 15 A) decreases the ionization rates at 125 eV. The HHG flux is additionally reduced by the macroscopic phase-mismatch between the generated harmonics and the driving laser. As the discharge raises the level of ionization, the free-electron density gradually increases leading to shorter coherence lengths for harmonics near 125 eV generated at lower ionization levels. In contrast, the higher energy harmonics around ~225 eV are generated at similar ionization levels, high above the initial Z_m, with or without the discharge preionization, and therefore have similar coherence lengths in both cases.

The hydrodynamic/atomic physics model confirms the enhancement of high photon energy harmonics in a capillary discharge is due to the formation of a pre-ionized medium, which can better withstand ionization-induced refraction. Also, a number of other interesting

observations, including enhanced waveguiding characteristics and reduced self-phase modulation (SPM) of the driving laser pulse, can be better understood in light of these simulation results, and are discussed below.

B. Self-Phase Modulation and Blueshift

An interesting feature of the data is the fact that the fundamental spectra (Fig. 9a) exhibits a blueshift that is reduced with higher discharge currents. This blueshift is caused by the rapid change of the index of refraction that accompanies fast ionization of the gas on the leading edge of the laser pulse. This ionization-induced blueshift is extremely large (~20 nm) for a hollow capillary filled with 5.2 Torr Ar, but is reduced to 6–15 nm when the discharge preionizes the gas. This reduced blueshift in the presence of the discharge is because without the discharge, neutral Ar is doubly ionized on the leading edge of the intense laser pulse. However, when the discharge is used to pre-ionize the medium, the laser only ionizes Ar^{+} to Ar^{2+}. This leads to a smaller index change during the rising edge of the laser pulse and, consequently, to reduced blueshifting of the emitted harmonics (Fig 9b). Thus, this effect can be distinguished from the blueshift induced by the intrinsic phase accumulated by the electron as it propagates in the laser field. Since an increase in the discharge current causes an increased level of ionization (Fig. 7e), the observed blueshift decreases with discharge current, as seen in both Figs. 9a and 9b. Fig. 9b shows the harmonic spectrum in the range of the 47^{th} harmonic for several discharge currents. The 47th harmonic with no discharge current present is blueshifted by 3.2 eV, which shifts this harmonic to approximately the wavelength corresponding to the 49^{th} harmonic in the presence of a discharge current of 25 A. In contrast, the shift in the 47^{th} harmonic at this discharge current is only 1.1 eV. The observed blueshift for currents between 0-25 A is between these two values. A

practical consequence of this effect is that it is possible to tune the harmonic wavelength by changing the discharge current to tailor the amount of blueshift.

C. Plasma guiding regimes

The capillary discharge not only reduces ionization-induced defocusing and self-phase modulation of the driving laser by creating a preformed, ionized medium, but, under certain conditions, it also creates a density profile that constitutes an index waveguide. Fig. 10 shows the measured transmission of ~28 fs FWHM, 8.5 mJ pulses through the waveguide initially filled with 6 Torr of Ar for different time delays between the rise of the current pulse and the injection of the laser pulse. The discharge was operated with conditions nearly identical to those that optimize HHG in Ar. Without the discharge the transmission is ~24 %, while the DC simmer current improves the transmission to 32%. When the current pulse is initiated, the transmission quickly rises to a peak pulse energy transmission of 65%. This is an improvement of the transmission efficiency of nearly a factor of 3. This high transmission remains relatively constant for approximately 1 μs and is high at the time delay where the best harmonic emission was observed.

In addition to this improvement of the overall transmission, the quality of the laser mode exiting the capillary is also significantly improved. Fig. 11 shows the spatial profiles of high intensity laser pulses in the exit plane of the capillary for several delays with respect to the onset of the current pulse. The profile of the laser pulse injected 0.1 μs before the rise of the discharge current fills the entire capillary bore and is heavily structured due to the high level of laser induced-ionization of neutral Ar. The images of the beam exiting the waveguide do not change significantly until about τ =0.5 μs after the initiation of the discharge. At τ =1.5 μs, the profile

has clearly become concentrated on the axis of the capillary with a diameter of approximately 150 um and the energy transmission efficiency was 65%.

Although the discharge significantly increases the transmission of intense pulses and dramatically improves the quality of the mode, it does not form an index waveguide under these discharge conditions in Ar. As the model results in Fig. 7 show, at the currents corresponding to these experiments the discharge does not form a concave electron density profile. The electron density is essentially uniform in the central region of the capillary, and the guiding is provided by the capillary walls. This is confirmed by Fig. 12, which shows near-field images of low intensity ($<10^{14}$ W/cm^2) laser pulses exiting the capillary at times prior to and during the discharge current pulse. At this low intensity the laser does not ionize the plasma significantly, and therefore there is no ionization-induced defocusing. There is very little change in the size and quality of the transmitted laser mode. This, in combination with the calculated electron density profile, leads us to conclude that, under these conditions the discharge, does not produce an index waveguide, and the enhanced transmission and mode quality is primarily due to reduced ionization-induced refraction. Higher discharge currents and higher initial pressures do lead to the creation of an index guide. However, as seen in Fig. 5, the low photon energy (i.e. 125eV) HHG decreases at higher levels of ionization due to reduced photoionization and shorter coherence lengths. The enhancement of the harmonic signal in Ar, shown in Fig. 2, is primarily due to the increased driving laser intensity from the reduction of ionization-induced defocusing associated with the preformed, ionized medium.

In contrast, the discharge does produce a Xe plasma with a concave density profile, as shown in Fig. 6d. The guided spot radius calculated from this profile is ≈82 μm, which is nearly the same as the spot size that is guided by the hollow capillary alone. Nevertheless, the concave

electron density profile and the pre-ionized plasma maintain a higher laser intensity over a longer distance, leading to the large extension and enhancement of the HHG photon energies near cutoff.

V. Conclusions

The generation of high harmonics in a capillary discharge waveguide significantly extends the cutoff photon energy for high harmonic generation. In xenon and krypton, the cutoff is extended by a factor of ~2, from 70 eV in previous measurements, to 160 eV and 170 eV, respectively. In Ar we observed photons of up to 275 eV, compared with past measurements that observed photons with energy up to 250 eV from Ar ions in waveguides without a discharge present. The discharge plasma can be tailored to have a very high degree of ionization (e.g. Ar^{8+}, [18]), in which the ions present can withstand very high laser intensities. Moreover, under certain conditions, the concave electron density profile created by the discharge can guide a high intensity laser beam over long distances, allowing for a long interaction length between the driving laser and the nonlinear medium at high laser intensities. Additionally, a method for continuously tuning the wavelengths of individual harmonic peaks was demonstrated in a capillary discharge plasma that complements other approaches for tuning the harmonics using chirped driving laser pulses [30, 31]. By changing the discharge current, the amount of blueshift of the driving laser, and therefore the blueshift of the generated harmonics, can be tuned. These results were interpreted by comparison with a hydrodynamic/atomic physics model of the discharge plasma.

Our data shows that the major limiting factor that prevents the discharge technique from extending efficient high harmonic generation to photon energies > 275 eV in Ar is the increasing

phase mismatch between the generated harmonics and the driving laser in the presence of a highly ionized plasma. The wavevector mismatch increases approximately linearly with the degree of ionization and with the harmonic order in highly ionized plasmas [32]. In the present work, the coherence length of the high energy harmonics is a small fraction of the length of the interaction medium. It is therefore clear that for this technique to extend to higher photon energies and higher efficiency, methods for correcting the phase-mismatch must be implemented. In hollow waveguides, quasi-phase matching (QPM) techniques have been demonstrated that employ modulations in the surface of the hollow waveguides[33, 34] or alternatively a train of counterpropagating pulses [35]. These techniques should also be successful in a capillary discharge. In addition, mixing of the driving laser field with a co-propagating[36, 37] or counterpropagating [37] weak fields of longer wavelength is also predicted to give rise to phase-matched harmonic generation in pre-ionized plasmas.

This work was supported by the U.S. Department of Energy Chemical Sciences, Geosciences, and Biosciences Division of the Office of Basic Energy Sciences using the facilities of the NSF ERC for Extreme Ultraviolet Science and Technology under NSF Award No. 0310717.

References:

[1] M. Bauer, J. Phys. D **38**, R253 (2005).

[2] L. Miaja-Avila, C. Lei, M. Aeschlimann, J. L. Gland, M. M. Murnane, H. C. Kapteyn, and G. Saathoff, Phys. Rev. Lett. **97**, 113604 (2006).

[3] J. Itatani, J. Levesque, D. Zeidler, H. Niikura, H. Pépin, J. C. Kieffer, P. B. Corkum, and D. M. Villeneuve, Nature **432**, 867 (2004).

[4] N. L. Wagner, A. Wüest, I. P. Christov, T. Popmintchev, X. Zhou, M. M. Murnane, and H. C. Kapteyn, PNAS **103**, 13279 (2006).

[5] H. Hasegawa, E. Takahashi, J. , Y. Nabekawa, K. L. Ishikawa, and K. Midorikawa, Physical Review A **71**, 023407 (2005).

[6] R. A. Bartels, A. Paul, H. Green, H. C. Kapteyn, M. M. Murnane, S. Backus, I. P. Christov, Y. Liu, D. Atwood, and C. Jacobsen, Science **297**, 379 (2002).

[7] R. a. I. Tobey, M. E. Siemens, O. Cohen, M. M. Murnane, and H. C. Kapteyn, Optics Letters, to be published (2007).

[8] K. C. Kulander, K. J. Schafer, and J. L. Krause, in *Super-Intense Laser-Atom Physics*, edited by B. Piraux, A. L'Huillier, and K. Rzazewski (Plenum, New York, 1993), p. 95.

[9] S. Palaniyappan, I. Ghebregziabher, A. DiChiara, J. MacDonald, and B. C. Walker, (APS, 2006), p. 033403.

[10] J. Zhou, J. Peatross, M. M. Murnane, H. C. Kapteyn, and I. P. Christov, Physical Review Letters **76**, 752 (1996).

[11] Z. H. Chang, A. Rundquist, H. W. Wang, M. M. Murnane, and H. C. Kapteyn, Physical Review Letters **79**, 2967 (1997).

[12] E. Seres, J. Seres, and C. Spielmann, Applied Physics Letters **89**, 181919 (2006).

[13] T. Brabec, and F. Krausz, Reviews of Modern Physics **72**, 545 (2000).

[14] E. A. Gibson, A. Paul, N. Wagner, R. a. Tobey, S. Backus, I. P. Christov, M. M. Murnane, and H. C. Kapteyn, Physical Review Letters **92**, 033001 (2004).

[15] J. L. Krause, K. J. Schafer, and K. C. Kulander, Physical Review Letters **68**, 3535 (1992).

[16] H. M. Milchberg, C. G. Durfee III, and T. J. McIlrath, Physical Review Letters **75**, 2494 (1995).

[17] A. Butler, D. J. Spence, and S. M. Hooker, Physical Review Letters **89**, 185003 (2002).

[18] B. M. Luther, Y. Wang, M. C. Marconi, J. L. A. Chilla, M. A. Larotonda, and J. J. Rocca, Physical Review Letters **92**, 235002 (2004).

[19] Y. Wang, B. M. Luther, M. Berrill, M. Marconi, F. Brizuela, J. J. Rocca, and V. N. Shlyaptsev, Physical Review E **72**, 026413 (2005).

[20] D. J. Spence, A. Butler, and S. M. Hooker, J. Opt. Soc. Am. B **20**, 138 (2003).

[21] D. M. Gaudiosi, B. A. Reagan, T. Popmintchev, M. Grisham, M. Berrill, O. Cohen, B. C. Walker, M. M. Murnane, H. C. Kapteyn, and J. J. Rocca, Physical Review Letters **96**, 203001 (2006).

[22] C. G. Wahlström, J. Larsson, A. Persson, T. Starczewski, S. Svanberg, P. Salières, P. Balcou, and A. L'Huillier, Physical Review A **48**, 4709 (1993).

[23] N. A. Papadogiannis, C. Kalpouzos, E. Goulielmakis, G. Nersisyan, D. Charalambidis, F. Augé, F. Weihe, and P. Balcou, Applied Physics B **73**, 687 (2001).

[24] M. V. Ammosov, N. B. Delone, and V. P. Krainov, Soviet Physics JETP **64**, 1191 (1986).

[25] M. Berrill, and J. J. Rocca, (unpublished)).

[26] M. F. Gu, The Astrophysical Journal **582**, 1241 (2003).

[27] H. Simmons, ADAD Manual V2.6 **http://adas.phys.strath.ac.uk/**.

[28] J. P. Apruzese, Journal of Quantitative Spectroscopy and Radiative Transfer **25**, 419 (1981).

[29] A. L. Lytle, X. Zhang, J. Peatross, M. M. Murnane, H. C. Kapteyn, and O. Cohen, Physical Review Letters **98**, 123904 (2007).

[30] H. T. Kim, D. G. Lee, K.-H. Hong, J.-H. Kim, I. W. Choi, and C. H. Nam, Physical Review A **67**, 051801 (2003).

[31] Z. Chang, A. Rundquist, H. Wang, I. Christov, H. C. Kapteyn, and M. M. Murnane, Physical Review A **58**, R30 (1998).

[32] C. G. Durfee, A. R. Rundquist, S. Backus, C. Herne, M. M. Murnane, and H. C. Kapteyn, Physical Review Letters **83**, 2187 (1999).

[33] E. A. Gibson, A. Paul, N. Wagner, R. Tobey, D. Gaudiosi, S. Backus, I. P. Christov, A. Aquila, E. M. Gullikson, D. T. Attwood, M. M. Murnane, and H. C. Kapteyn, Science **302**, 95 (2003).

[34] A. Paul, R. A. Bartels, R. Tobey, H. Green, S. Weiman, I. P. Christov, M. M. Murnane, H. C. Kapteyn, and S. Backus, Nature **421**, 51 (2003).

[35] X. Zhang, A. L. Lytle, H. C. Kapteyn, M. M. Murnane, and O. Cohen, Nature Physics, to be published (2007).

[36] P. L. Shkolnikov, A. E. Kaplan, and A. Lago, Optics Letters **18**, 1700 (1993).

[37] O. Cohen, T. Popmintchev, D. M. Gaudiosi, M. M. Murnane, and H. C. Kapteyn, Physical Review Letters **98**, 043903 (2007).

Figure Caption List:

FIG. 1. Schematic of the experimental setup. The inset is a diagram of the capillary discharge.

FIG. 2. (Color online) High-order harmonic spectra on a log scale with (solid red) and without (dashed black) the discharge showing an extension of the HHG cutoff to photon energies of: (a) above 160 eV in 3 Torr of Xe using 10 mJ laser pulses; (b) above 170 eV in 6 Torr of Kr with 10 mJ laser pulses; and (c) above 275 eV in 6 Torr of Ar with 11 mJ laser pulses. A 250 um diameter bore, hollow core fiber was used for all three gases. The discharge current and the time delay parameters are shown in the picture.

FIG. 3. (Color online) HHG signal for various delay times τ between the onset of the discharge current pulse and the injection of the laser pulse (dotted blue τ=-1μs, laser pulse arrives before the current pulse; solid red τ=2μs, optimal time delay; dash-dot green τ=6 μs, laser pulse arrives after the current pulse). The spectra were obtained from 6 Torr of Ar using 9 mJ, 28 fs laser pulses in the capillary discharge with 5 A current pulses. A spectrum obtained under the same conditions in a hollow waveguide (dashed black) is shown for comparison.

FIG. 4. (Color online) Laser intensity dependence of the highest observed photon energies obtained from 6 Torr of Ar using 9 mJ and 11 mJ, 28 fs pulses, injected 2 μs after a current pulse of 5 A. The HHG spectra extend towards higher energies when laser intensity is increased in the case of a capillary discharge while the highest observed photon energies are intensity independent when a hollow waveguide is used.

FIG. 5. (Color online) Harmonic emission from 6 Torr of Ar using 11 mJ, 28 fs laser pulses and various peak discharge currents: 5 A (solid red), 10 A (dotted blue), 15 A (dash-dot green), and no discharge (dashed black). Each spectrum was measured at a delay of τ=2μs. The HHG signal decreases at lower harmonic orders and remains the same at high harmonic orders. The increasing electron density with current leads to further reduction of the coherence lengths.

FIG. 6. (Color online) Calculated discharge plasma parameters for the measured 10 A current pulse (a) in a 250 um inner diameter capillary initially filled with 3.0 Torr Xe. The mean ion charge (b) of the plasma is Z_m~1 over most of the radius for most of the current pulse. The electron temperature (c) is highest on axis and decreases radially giving rise to a concave transverse electron density profile (d) through pressure equilibrium. The electron density profile at 2000 ns is plotted in (e). Please see the online version for an accurate color scale.

FIG. 7. (Color online) Calculated discharge plasma parameters for a 10 A current pulse in a 250 um inner diameter capillary initially filled with 6.0 Torr Ar. The mean ionization (a) of the plasma peaks at Z_m=.6. The electron temperature (b) and the electron density profile (c) are significantly different than in the case of Xe. The electron density profile at 1500 ns (d) is essentially flat over the radius of the capillary. (e) Model prediction of peak mean ion charge vs. discharge current for an initially 6.0 Torr Ar plasma in a 250 μm capillary. Please see the online version for an accurate color scale.

Fig. 8. (Color online) Calculated mean ionization Z_m and laser ionization rates of Ar species for 28 fs laser pulses with peak intensities of 1.3 10^{15} W/cm^2, (a) and (b), and 2.3 10^{15} W/ cm^2, (c) and (d), using ADK rates for the conditions in Fig. 5 (without the discharge (solid red, initial Z_m=0); with a discharge current of 5 A (dashed blue, initial Z_m~0.3) and 15 A (solid green, initial Z_m~1)). The right axes show the predicted threshold photon energy for the laser intensity profile (dotted black) calculated from the cutoff rule $h\nu_{max} = I_p + 3.17U_p$.

FIG. 9. (Color online) (a) Spectra showing the blueshift of 9 mJ laser pulses for various currents in the capillary discharge initially filled with 5.2 Torr Ar. The spectra for discharge currents of 0 A, 10 A, 20 A, and 30 A, and through an evacuated capillary are shown with central wavelengths (vertical bars) of 773 nm, 778 nm, 784 nm, 787 nm, and 793 nm, respectively. (b) High harmonic spectra, from a 9 mJ pulse propagating through 5.8 Torr Ar, with and without the discharge present, showing the effects of blueshifting of the fundamental spectrum. Spectra for 0 A, 10 A, 20 A, and 25 A are shown, as is the location of the center of the 47th harmonic (vertical bars).

FIG. 10 (Color online). Measured transmission (stars) of 8.5 mJ, 28 fs FWHM pulses through the 5 cm capillary discharge waveguide with a 10 A peak current pulse and an initial Ar pressure of 6.0 Torr. The measured current pulse is shown.

FIG. 11. (Color online) Near field images of intense laser pulses in the exit plane of the capillary at different time delays during the current pulse. The initial Ar pressure was 6.0 Torr and 10 A current pulses were used. The input laser pulses were 28 fs FWHM in duration and had energies of 8.5 mJ.

FIG. 12. (Color online) Comparison of near field images of low intensity ($<10^{14}$ W/cm^2) laser pulses exiting the discharge at (a) 200 ns before the onset of the current pulse, (b) 600 ns and (c) 1200 ns after the onset of the current pulse. The discharge was operated under the same conditions as in Fig. 11.

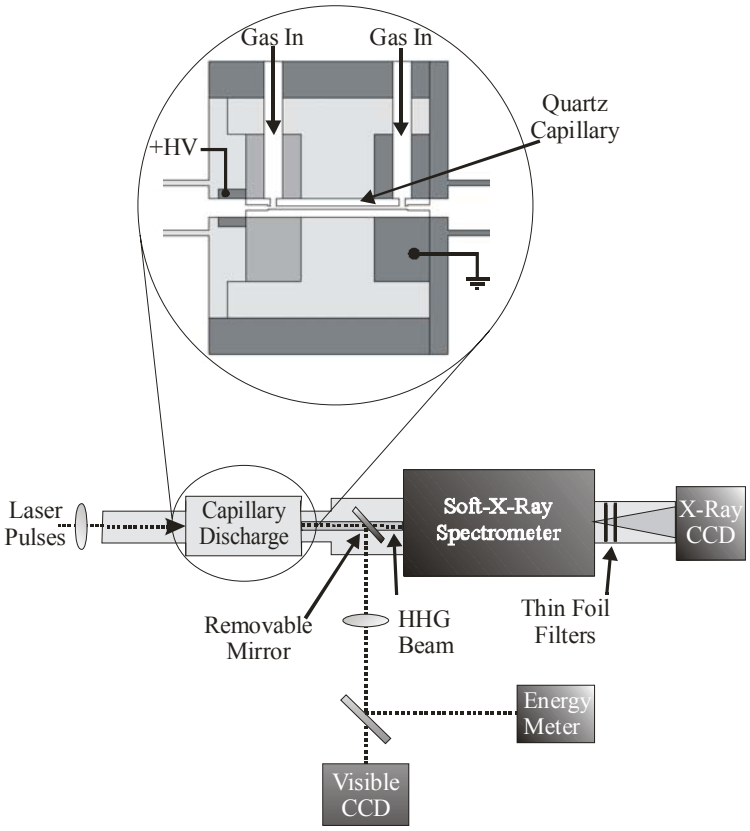
Gas In
Gas In
Quartz
Capillary
+HV
Laser
Pulses
Capillary
Discharge
Soft-X-Ray
Spectrometer
X-Ray
CCD
Removable
Mirror
HHG
Beam
Thin Foil
Filters
Energy
Meter
Visible
CCD

FIG. 1

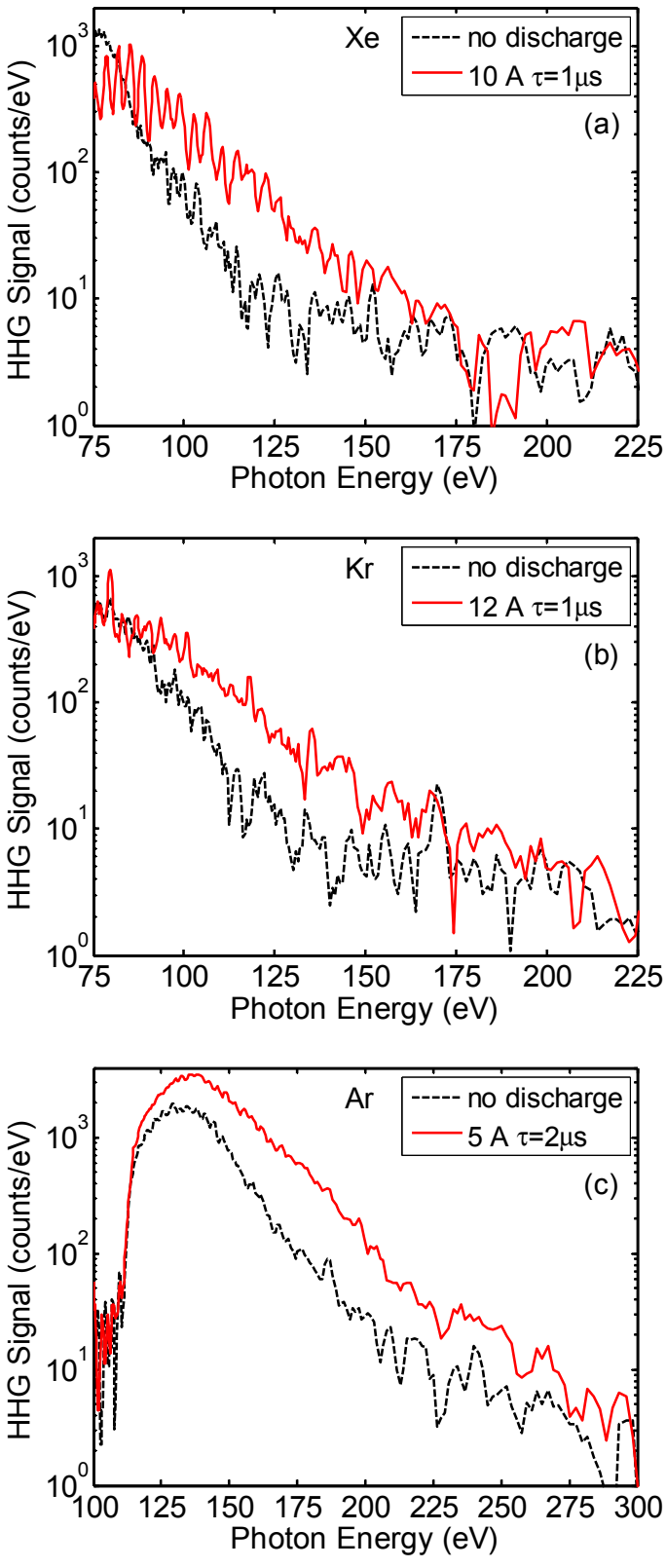
Xe
----- no discharge
10 A τ=1μs
(a)
HHG Signal (counts/eV)
Photon Energy (eV)
Kr
----- no discharge
12 A τ=1μs
(b)
HHG Signal (counts/eV)
Photon Energy (eV)
Ar
----- no discharge
5 A τ=2μs
(c)
HHG Signal (counts/eV)
Photon Energy (eV)

FIG. 2

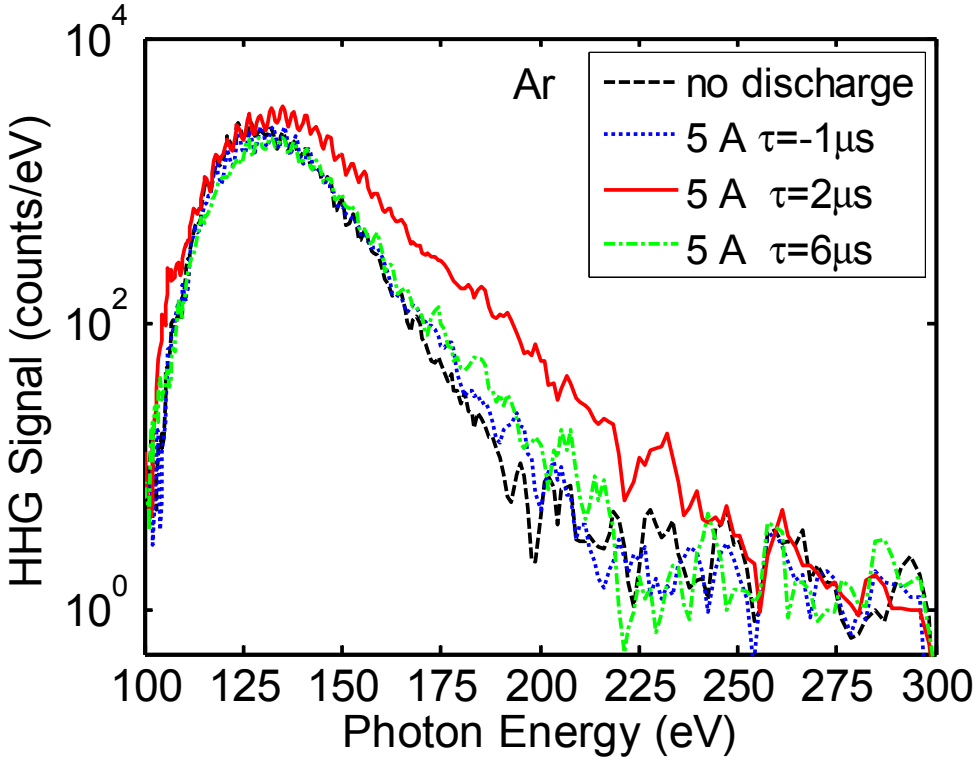
Ar
no discharge
5 A τ=-1μs
5 A τ=2μs
5 A τ=6μs
HHG Signal (counts/eV)
Photon Energy (eV)
10^4
10^2
10^0
100 125 150 175 200 225 250 275 300

FIG. 3

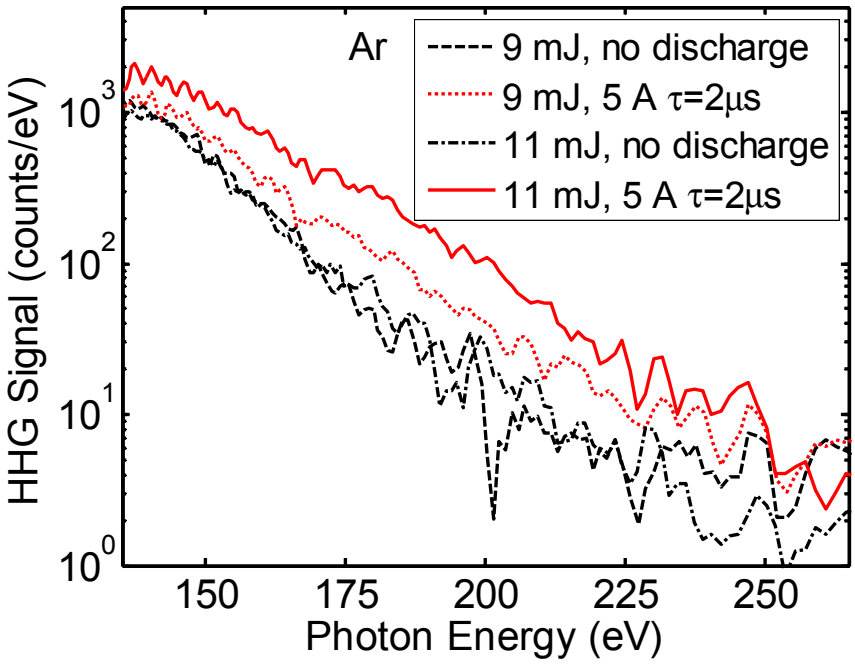
Ar
9 mJ, no discharge
9 mJ, 5 A τ=2μs
11 mJ, no discharge
11 mJ, 5 A τ=2μs
HHG Signal (counts/eV)
10^3
10^2
10^1
10^0
150
175
200
225
250
Photon Energy (eV)

FIG. 4

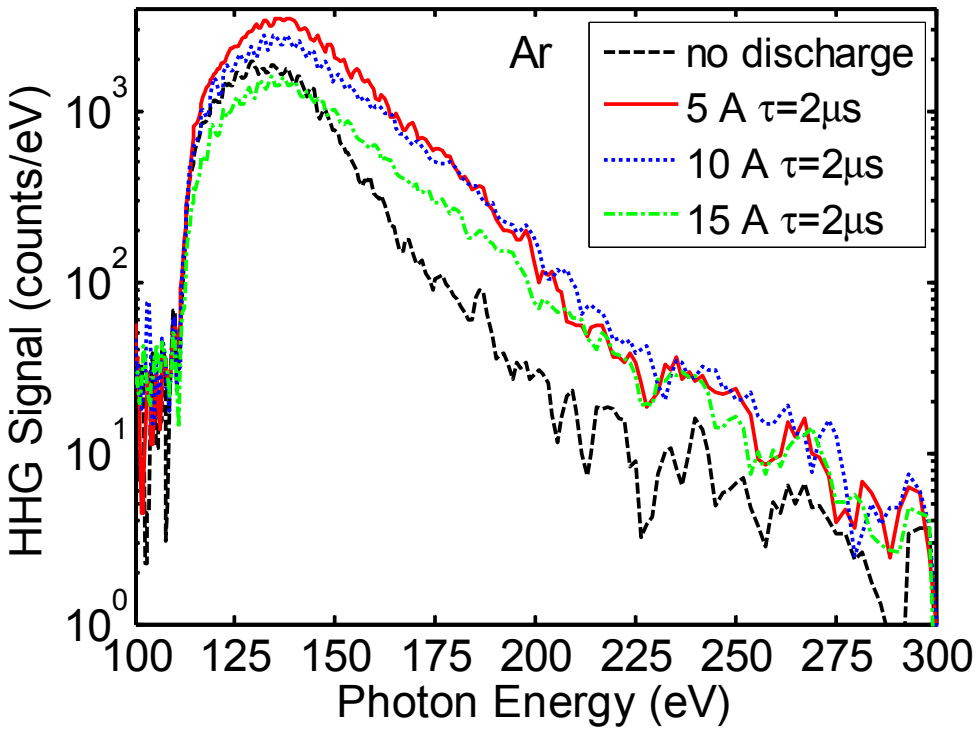
Ar
no discharge
5 A τ=2μs
10 A τ=2μs
15 A τ=2μs
HHG Signal (counts/eV)
Photon Energy (eV)
10^0
10^1
10^2
10^3
100
125
150
175
200
225
250
275
300

FIG. 5

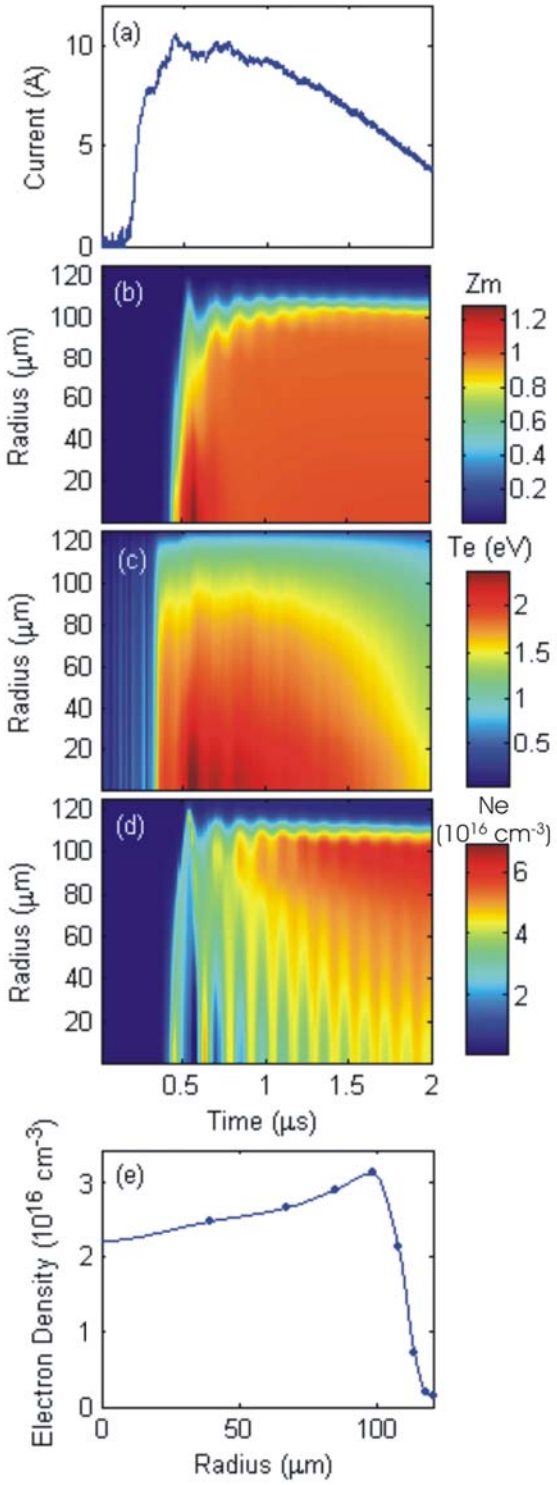
(a)
Current (A)
10
5
0
(b)
Radius (μm)
120
100
80
60
40
20
Zm
1.2
1
0.8
0.6
0.4
0.2
(c)
Radius (μm)
Te (eV)
2
1.5
1
0.5
(d)
Radius (μm)
Ne
(10^16 cm^-3)
6
4
2
0.5
1
1.5
2
Time (μs)
(e)
Electron Density (10^16 cm^-3)
3
2
1
0
0
50
100
Radius (μm)

FIG. 6

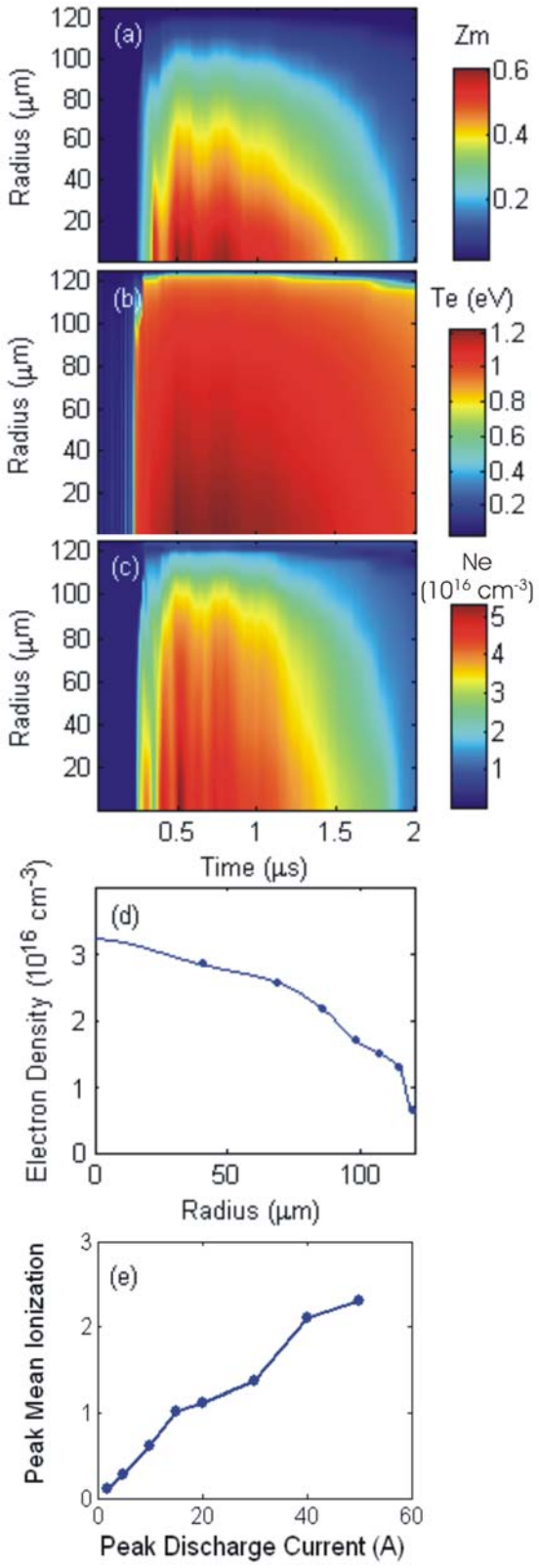
(a)
(b)
(c)
(d)
(e)
Radius (μm)
Zm
Te (eV)
Ne
(10^16 cm^-3)
Time (μs)
Electron Density (10^16 cm^-3)
Radius (μm)
Peak Mean Ionization
Peak Discharge Current (A)

FIG. 7

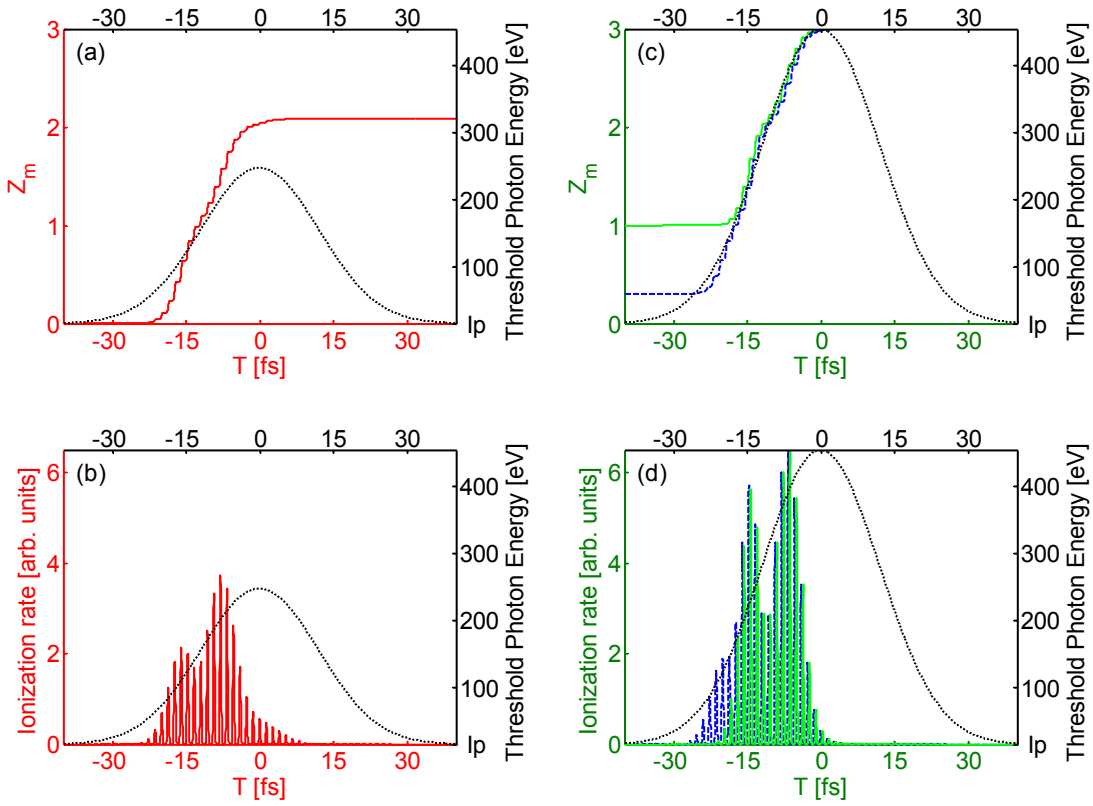
(a)
(b)
(c)
(d)
Z_m
Ionization rate [arb. units]
T [fs]
Threshold Photon Energy [eV]
Ip
-30
-15
0
15
30
0
1
2
3
4
6
100
200
300
400

FIG. 8

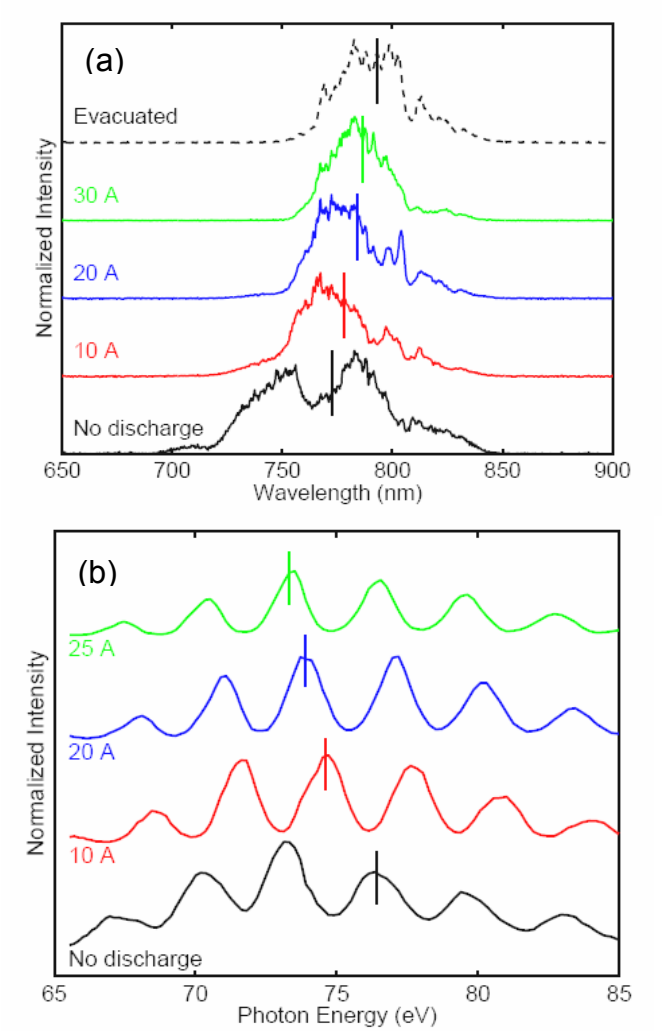
(a)
Evacuated
30 A
20 A
10 A
No discharge
Normalized Intensity
650
700
750
800
850
900
Wavelength (nm)
(b)
25 A
20 A
10 A
No discharge
Normalized Intensity
65
70
75
80
85
Photon Energy (eV)

FIG. 9

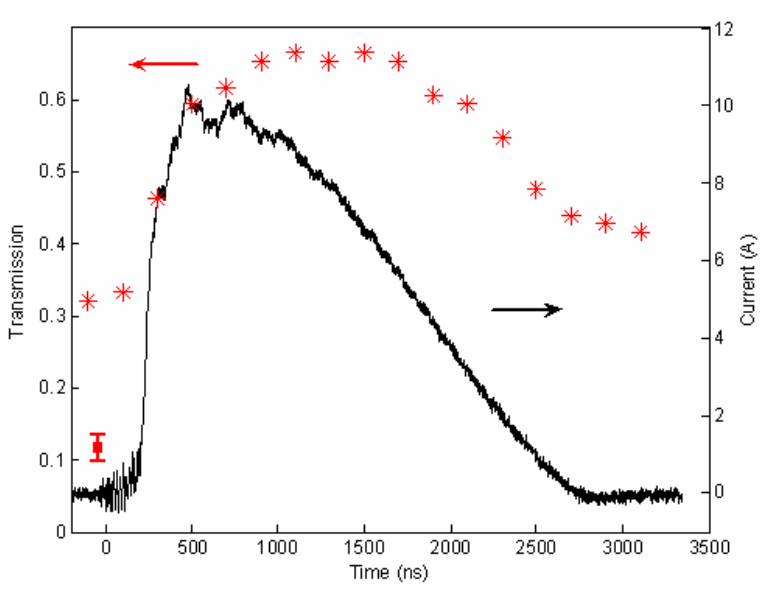
Transmission
Current (A)
Time (ns)
0
0.1
0.2
0.3
0.4
0.5
0.6
0
2
4
6
8
10
12
0
500
1000
1500
2000
2500
3000
3500

FIG. 10

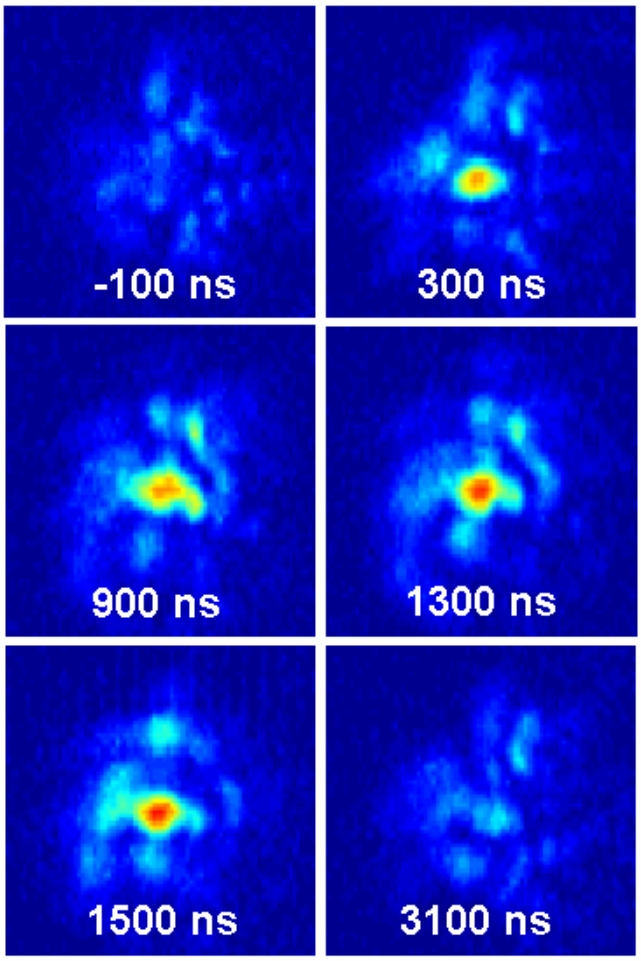

FIG. 11

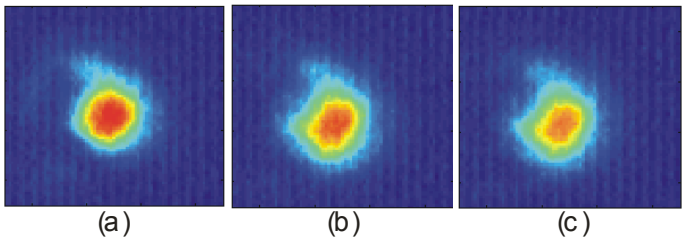

FIG. 12